Langmuir

Article

pubs.acs.org/Langmuir

Effects of Adsorbed Pyridine Derivatives and Ultrathin Atomic-Layer-Deposited Alumina Coatings on the Conduction Band-Edge Energy of TiO_2 and on Redox-Shuttle-Derived Dark Currents

Michael J. Katz,[†] Michael J. D. Vermeer,[†,‡] Omar K. Farha,[†] Michael J. Pellin,[†,‡] and Joseph T. Hupp*[,†,‡,§]

[†]Department of Chemistry and Argonne-Northwestern Solar Energy Research (ANSER) Center, Northwestern University, 2145 Sheridan Road, Evanston, Illinois 60208, United States

[‡]Materials Science Division and [§]Chemical Sciences and Engineering Division, Argonne National Laboratory, 9700 South Cass Avenue, Argonne, Illinois 60439, United States

ABSTRACT: Both the adsorption of *t*-butylpyridine and the atomic-layer deposition of ultrathin conformal coatings of insulators (such as alumina) are known to boost open-circuit photovoltages substantially for dye-sensitized solar cells. One attractive interpretation is that these modifiers significantly shift the conduction-edge energy of the electrode, thereby shifting the onset potential for dark current arising from the interception of injected electrons by solution-phase redox shuttle components such as Co(phenanthroline)$_3^{3+}$ and triiodide. For standard, high-area, nanoporous photoelectrodes, band-edge energies are difficult to measure directly. In contrast, for flat electrodes they are readily accessible from Mott–Schottky analyses of impedance data. Using such electrodes (specifically TiO_2), we find that neither organic nor inorganic electrode-surface modifiers shift the conduction-band-edge energy sufficiently to account fully for the beneficial effects on electrode behavior (i.e., the suppression of dark current). Additional experiments reveal that the efficacy of ultrathin coatings of Al_2O_3 arises chiefly from the passivation of redox-catalytic surface states. In contrast, adsorbed *t*-butylpyridine appears to suppress dark currents mainly by physically blocking access of shuttle molecules to the electrode surface. Studies with other derivatives of pyridine, including sterically and/or electronically diverse derivatives, show that heterocycle adsorption and the concomitant suppression of dark current does not require the coordination of surface Ti(IV) or Al(III) atoms. Notably, the favorable (i.e., negative) shifts in onset potential for the flow of dark current engendered by organic and inorganic surface modifiers are additive. Furthermore, they appear to be largely insensitive to the identity of shuttle molecules.

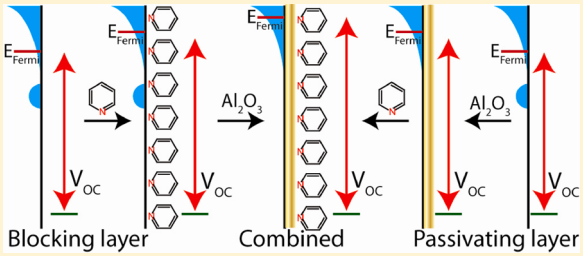

INTRODUCTION

Dye-sensitized solar cells (DSCs) constitute a promising technology for light to electrical-energy conversion.[1−6] The basic DSC operational scheme is as follows: (1) A dye molecule adsorbed on a high-surface-area porous nanoparticle semiconductor array absorbs light. (2) The excited state of the dye injects an electron into the conduction band of the semiconductor; the electron then diffuses through the array and is collected at the substrate. (3) The oxidized dye is regenerated by a redox shuttle in solution. (4) The redox shuttle is regenerated at the dark electrode.

The archetypal cell utilizes a Ru-based dye,[7] typically N719 (i.e., ditetrabutyl-ammonium *cis*-bis(isothiocyanato)-bis(2,2′-bipyridyl-4,4′-dicarboxylato)ruthenium(II)[8,9]). The semiconductor nanoparticles are most often TiO_2, and the redox shuttle is most often the I_3^-/I^- couple.[5] For a fully optimized cell with this composition, the small-scale/laboratory efficiency is approximately 11.5% at 1 sun, but the theoretical limit of the DSC is significantly higher.[10,11] (The highest efficiency, multidye, single-photoelectrode cells deliver 12.3% at 1 sun.[12]) Beneficial pathways for charge transfer and charge transport necessarily compete with detrimental pathways, resulting in a host of kinetic and thermodynamic issues in cell operation. These issues can influence both photovoltages and photocurrents and thereby directly affect efficiencies.[3,13,14] For example, N719 has an optical band gap of 1.6 eV,[8,11] yet near-champion DSCs as described above achieve voltages of only ca. 0.8 V. Thus, nearly half of the hypothetical maximum open-circuit photovoltage (V_{oc}) is lost. Some of the lost voltage is used by the cells to ensure that electron-transfer steps are effectively irreversible; these losses would be difficult to recover even with ideally performing cell components.[11,14,15] Others are consequences of a slow forward reaction or transport kinetics, the coupling of charge transfer to chemical steps, the catalysis of back-reaction structural defects, and so on. These, in principle, can be recovered via cell component replacement or modification.

As shown in Figure 1, V_{oc} is equal to the difference between the Nernstian potential of the redox shuttle (the potential of the dark electrode) and the quasi-Fermi level, E_{Fermi}, of the dye-coated electrode. Although there are often complications, in practice the potential of the dark electrode can in principle be

Received: October 5, 2012
Revised: December 14, 2012
Published: December 17, 2012

   dx.doi.org/10.1021/la303962y | *Langmuir* 2013, 29, 806−814

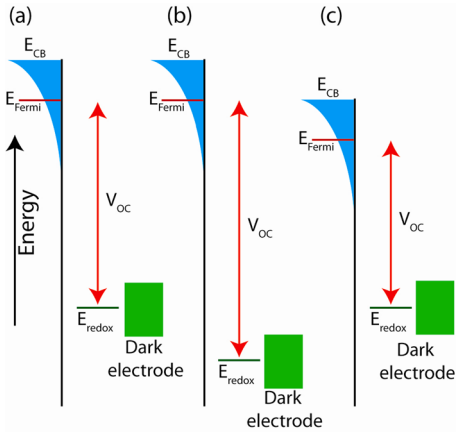

Figure 1. (a) V_{oc} of a DSC is the difference between the Nernstian potential of the redox shuttle and E_{Fermi} of the semiconductor. (b) Changing the redox shuttle to one having a more positive electrochemical potential increases V_{oc}. (c) The addition of potential-determining cations or other solution components can lower V_{oc} by lowering E_{cb} and hence E_{Fermi}. Note that the sign convention for electrochemical potentials is the reverse of that for absolute energies versus vacuum (i.e., an energy of zero for an electron in vacuum). Thus, electrochemical potentials become more positive as one moves downward along the energy axis, whereas absolute energies become more negative.

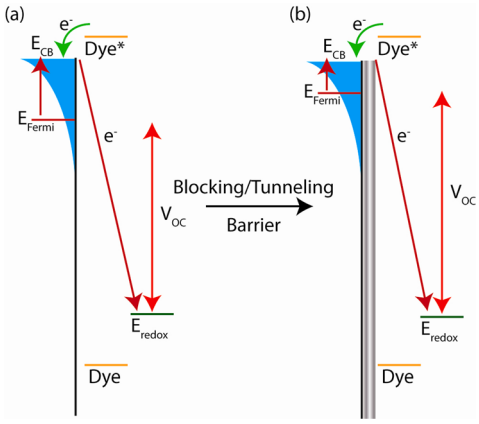

Figure 2. Adding a blocking/tunneling barrier to an electrode surface slows interfacial electron transfer and increases E_{Fermi} and thus V_{oc}.

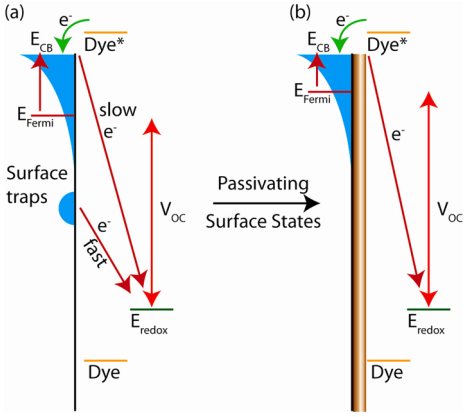

Figure 3. Passivating the redox-catalytic surface states of an electrode, thus increasing E_{Fermi} and V_{oc}.

readily and systematically altered by changing the chemical identity and therefore the formal potential of the redox shuttle (Figure 1b).[16−26] The potential of the illuminated electrode can be adjusted by shifting the electrode's conduction-band-edge energy, E_{CB}, for example, by introducing so-called potential-determining cations such as Li^+ or H^+ to the cell solution (Figure 1c).[27−29]

The open-circuit potential, of course, is also the potential at which the anodic photocurrent (arising from dye injection and subsequent charge collection) is precisely offset by the potential-dependent flow of current in the reverse direction (i.e., current due to the interception of injected electrons by the redox shuttle or the recombination of injected electrons with the oxidized dye). Typically, interception is considerably more important than recombination; thus, current flow in the reverse direction can often be well approximated by measuring the current at the semiconductor electrode under dark conditions. Consequently, additives that suppress the potential-dependent dark current, either by creating a blocking layer (tunneling barrier) to electron interception or by passivating electrode surface states that facilitate electron interception, will generally raise the quasi-Fermi level of the illuminated electrode and increase the DSC photovoltage and energy-conversion efficiency. Figures 2 and 3 illustrate these two possibilities.

Among the many additives/surface modifiers that have been evaluated for their ability to suppress dark current and boost photovoltages are adsorbed *t*-butylpyridine (tbp)[8,28,30−33] and ultrathin, insulating metal oxide layers,[19,34−41] especially well-defined conformal layers constructed via atomic layer deposition (ALD).[19,23,34,37,42,43] Although tbp is thought to suppress dark currents mainly by shifting E_{cb},[28,32,33] other effects may also be important. For ALD-formed insulating layers, evidence exists (mainly with nanoparticulate SnO_2 electrodes)[37] to support the mechanisms illustrated in both Figures 2 and 3. Nevertheless, it has been suggested that the displacement of E_{cb} (i.e., the mechanism in Figure 1c) is also important.[40]

One means of testing the E_{cb}-shift notion would be to measure electrode flat-band potentials (E_{fb}) before and after treatment with molecules or materials known to suppress dark currents and alter V_{oc}. For an n-type semiconductor, the flat-band potential is closely related to the conduction-band-edge energy. Unfortunately, the standard experimental approach to assessing E_{fb}, the Mott−Schottky assessment of electrochemical capacitance data,[44−46] is not applicable to porous electrodes (such as the high-area nanoparticulate photoelectrodes typically used in DSCs).[47,48] We reasoned, however, that ALD could be used to fabricate nonporous (flat) TiO_2 electrodes and that these in turn could be evaluated via the Mott−Schottky method. Below we report on the effects of molecular adsorbates and ALD-formed insulating layers on E_{fb} and E_{cb}. From these and related experiments, we have obtained insights into the mechanisms by which these modifiers alter the photoelectrode performance. Additionally, from dopant-density information yielded by the experiments, we have obtained insight into the behavior of ALD-TiO_2 electrodes previously examined in other contexts.[49,50]

EXPERIMENTAL SECTION

Fluorine-doped tin oxide-coated (FTO-coated) glass (8 Ω cm^{-2}) was purchased from Hartford Glass. Unless otherwise stated, all other reagents were acquired from commercial sources and used without

dx.doi.org/10.1021/la303962y | *Langmuir* 2013, 29, 806−814

further purification. $[Co(1,10\text{-phenanthroline})_3](ClO_4)_3$ ($Co(phen)_3^{3+}$) was made according to a literature procedure.[43] 2,6-Diphenylpyridine was synthesized via literature procedures.[51]

Electrode Preparation. Squares of dimensions 2.0 × 2.0 cm^2 were cut from an FTO-coated glass sheet. Each sample was sonicated in water with detergent for 15 min, washed with deionized water, sonicated in isopropanol for 15 min, sonicated with methanol for 15 min, and finally held at 500 °C for 1 h.

Flat TiO_2 films were synthesized by atomic-layer deposition in a Savannah 100 reactor made by Cambridge Nanotech Inc. Films were prepared using alternating cycles of titanium tetra-isopropoxide (0.1 s pulse, 1 s exposure, 10 s nitrogen purge) and deionized water (0.1 s pulse, 1 s exposure, 15 s nitrogen purge).[52,53] The reactor temperature was maintained at 200 °C, and the titanium tetra-isopropoxide reservoir was maintained at 80 °C. The TiO_2 growth rate (previously measured in our laboratory on silicon using ellipsometry) is 0.35 Å/cycle. Alternating cycles (900) of the precursors were deposited, yielding a film ca. 32 nm thick. Prior to any further ALD process or experimentation, the films were annealed at 500 °C for an hour to ensure that the initially amorphous films were crystallized as the metastable anatase phase.[54]

Alumina coatings were grown on annealed TiO_2 films by using three ALD cycles, each consisting of a 0.1 s pulse and 1 s exposure to trimethylaluminum, a 30 s purge, and a 0.1 s pulse and 1 s exposure to water vapor. For each electrode, an edge was sanded to expose FTO. Silver epoxy was then spread on the exposed section to enable external electrical contact. A piece of 25 μm Surlyn with a 0.25 cm^2 hole was melted onto the film surface at 140 °C in order to define a fixed active area for each electrode.

Electrochemical Measurements. All electrochemical measurements were made on a Solartron Analytical Modulab instrument equipped with a 1 MHz frequency analyzer and a potentiostat capable of measuring 1 million samples/s. A Ag/AgCl reference electrode in saturated KCl(aq) and a platinum mesh counter electrode were used. All electrochemical experiments were three-electrode experiments. The stability of the reference electrode was monitored between experiments by recording cyclic voltamograms of ferrocene in acetonitrile containing tetrabutylammonium tetrafluoroborate as a supporting electrolyte. No shifts in the potential of the reference electrode versus the ferrocene formal potential were observed over the course of the experiments.

Electrochemical impedance spectroscopy was performed with solutions consisting of 0.2 M $LiClO_4$ in acetonitrile, with or without 0.2 M tbp. The potential was stepped from −500 to −750 mV in 25 mV increments. A 10 mV sinusoidal signal was utilized as the perturbation over a 500 kHz to 0.05 Hz range. For dark current and open-circuit voltage decay measurements, the potential was swept from 100 to −850 mV at 50 mV/s while monitoring the current. The potential was then fixed at −850 mV for 10 s. Potentiostatic control then ceased, and the voltage decay was recorded as a function of time (1000 points/s). The electrolyte consisted of either 0.02 M $Co(phen)_3^{3+}$ or 0.02 M LiI_3 in 0.2 M $LiClO_4$, with or without 0.2 M pyridine or a derivative.

RESULTS AND DISCUSSION

Band-Edge Energetics. The Mott−Schottky treatment of the potential-dependent distribution of free charges within a semiconductor electrode in contact with an electrolyte solution provides a basis for extracting the flat-band potential from experimental measurements of an electrode's capacitance. The Mott−Schottky equation can be written as

$$\frac{A^2}{C^2} = \frac{2}{q\varepsilon\varepsilon_o N}\left(E - E_{FB} - \frac{kT}{q}\right) \quad (1)$$

where A is the solution-exposed surface area of the electrode, q is the charge of the electron, ε is the dielectric constant of the material, ε_o is the permittivity of free space, N is the donor density, E is the applied electrode potential, k is Boltzmann's constant, and T is temperature.[44,45] A Mott−Schottky plot (i.e., a plot of the inverse square of the area-normalized capacitance vs. electrode potential) should produce a straight line with an x intercept equaling the flat-band potential plus the thermal voltage, kT/q. The slope of the plot should vary inversely with the donor density.

Figure 4 shows the linear region of a plot of A^2C^{-2} versus E for an unmodified TiO_2 electrode in contact with 0.2 M $LiClO_4$

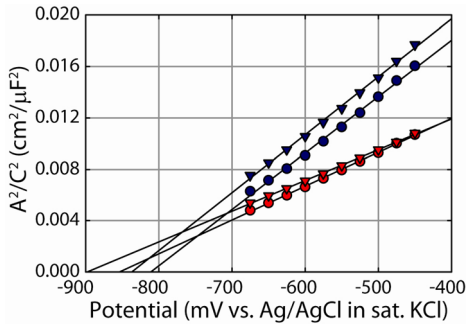

Figure 4. Mott−Schottky plots for flat TiO_2 electrodes, with (red triangles) and without tbp (red circles), and those treated with 3 ALD cycles of Al_2O_3 and run with (blue triangles) and without (blue circles) tbp.

in acetonitrile (red circles). After accounting for a kT/q value of 27 mV, we found that the extrapolated intercept of the plot yields an E_{fb} value of −880 mV versus a Ag/AgCl reference electrode. Repeat measurements with this electrode produced values that were reproducible to within ±5 mV. The statistical error over several electrodes was ±50 mV. The conduction band edge can be determined from the flat-band potential via eqs 2 and 3 [55]

$$E_{CB} = q\left(E_{FB} - \frac{kT}{q}\ln\frac{N_C^*}{N}\right) \quad (2)$$

$$N_C^* = \left(\frac{2\pi m_e^* kT}{h^2}\right)^{3/2} \quad (3)$$

where N_C^* is the effective density of electronic states and m_e^* is the effective mass of the electron, here taken to be ca. 1.8 times the electron's rest mass.[56] On this basis, E_{cb} is ca. −900 mV. After accounting for differences in reference electrodes, we find this value to be in reasonable agreement with results from previous studies in similar electrolytes.[57]

Repeating the impedance experiments in the presence of 0.2 M tbp yielded E_{fb} and E_{cb} values that are shifted to more negative potentials by only ca. 20−40 mV (Figure 4). Because tbp addition typically boosts open-circuit photovoltages by ca. 200 mV, we conclude that factors in addition to a simple shift in E_{cb} (Figure 1c, but in the opposite direction) are important in operational DSCs;[8,32,58−60] these possibilities are considered further in subsequent sections. The observed small shifts in E_{cb} and E_{fb} stand in contrast to much larger shifts inferred from Mott−Schottky experiments with high-area nanoparticulate electrodes (i.e., shifts of ca. −200 to −300 mV[59,61]). As noted above, however, the derivation of the Mott−Schottky relation entails assumptions that are unlikely to be met by porous, nanoparticulate electrodes.[48,62] Among the most tenuous assumptions for these electrodes are that (a) band bending is

dx.doi.org/10.1021/la303962y | Langmuir 2013, 29, 806−814

significant and (b) particle sizes and interparticle spaces are large compared to space-charge-layer thicknesses. It is conceivable that the failure to meet these conditions with nanoparticulate electrodes causes the Mott−Schottky experiments to report primarily on effects other than shifts in E_{cb}. Alternatively, it might be that nanoparticulate electrodes, derived from colloidal suspensions, are much more strongly influenced by added tbp than are electrodes grown by ALD from vapor-phase titanium tetra-isopropoxide and water. If, for example, colloid-derived nanoparticulate electrodes feature excess protonated surface sites, then tbp addition would likely neutralize or buffer these sites and shift the conduction-band edge negatively. The sensitivity of E_{cb} values for TiO_2 to pH is well established[63,64] and has been shown to extend over more than 30 pH units at ca. −60 mV/pH unit.[63] Perhaps significantly, the apparent E_{cb} values for high-area nanoparticulate electrodes,[59,61] derived from Mott−Schottky experiments, approach more closely the E_{cb} values for ALD-constructed electrodes (Figure 4) when tbp, a weak Brønsted base and potential buffer, is present.

Also shown in Figure 4 are Mott−Schottky plots for a flat TiO_2 electrode coated with ALD with a ca. 3 Å layer of insulating alumina. (To minimize batch-to-batch variations, the two electrodes examined in Figure 4 were prepared during the same TiO_2 ALD run.) Notably, the flat-band potential is shifted by only about 40 mV (and in the positive direction) relative to its value for an alumina-free electrode (i.e., comparable to the electrode-to-electrode measurement variability in the absence of surface modification[40]). This finding is consistent with our previous interpretation of ALD-insulator-layer effects on open-circuit photovoltages in DSCs primarily in terms of effects other than shifts in E_{cb}.[19,37,43,65] Also notable is the absence of a sizable effect of tbp on the flat-band potential. As with alumina-free TiO_2, the experiments reveal a shift of only about −30 mV.

The substantially differing slopes (factor of ∼1.7) for Mott−Schottky plots for ALD-coated versus ALD-free electrodes imply a substantially greater donor density for the latter (i.e., ca. 1.7-fold greater). Given that the electrodes examined in Figure 4 are roughly 30 nm thick and that the thickness of the alumina coating is only ∼0.3 nm, this interpretation is almost certainly incorrect. A more probable interpretation is that alumina passivates surface-localized states that can otherwise accept and release charge (electron density) as a function of the applied electrode potential and thereby contribute to the measured capacitance.[66] (Note that at each of the points shown in Figure 4 the measured capacitance is smaller (C^{-2} is larger) for the ALD-coated electrode.)

If we assume that the slopes of the Mott−Schottky plots for the alumina-coated electrodes do not include significant contributions due to surface states (a sensible assumption given the thermodynamic inaccessibility of the Al(III/II) couple in oxide environments), then the donor density within the flat electrodes is ca. 2×10^{19} m^{-3}. With this information, the potential-dependent thickness of the space-charge layer can be calculated from refs 46 and 55.

$$W = \sqrt{\frac{2\varepsilon\varepsilon_o \Delta E}{qN}} \tag{4}$$

In eq 4, ΔE is the potential drop across the semiconductor. Assuming a static dielectric constant for TiO_2 of 55,[61] the thickness of the space-charge layer is ∼12 nm at typical values of V_{oc} in iodide-containing DSCs and ∼25 nm at the I_3^-/I^- potential. We have proposed elsewhere[50] that band bending within ALD-formed TiO_2 electrodes featuring either nanotube[67] or cylindrical shell geometries[50] can slow back electron transfer to redox shuttles once the TiO_2 thickness reaches a few to several nanometers. The results obtained here support those proposals.

Dark Currents. Given the inability of tpb- or alumina-induced shifts in E_{cb} for flat TiO_2 electrodes to account fully for shifts in V_{oc} in operating DSCs (via the mechanism in Figure 1c), we extended our investigation to include the effects of these modifiers on dark currents. Shown in Figure 5 are the

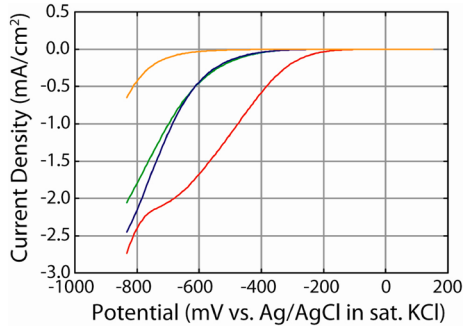

Figure 5. Dark-current-density measurements for flat TiO_2 electrodes using 0.02 M I_3^- as the electron interceptor. Key: unmodified electrode (red), after the addition of 0.2 M tbp (green), Al_2O_3-coated electrode with no tbp (blue), and Al_2O_3-coated electrode after the addition of 0.2 M tbp (orange).

results for flat-electrode cells containing 0.02 M I_3^- as the electron interceptor. The salient features are (a) a shoulder in the current−density (J) versus voltage curve for unmodified TiO_2, (b) a shift in the onset potential for I_3^- reduction by approximately −200 mV following the addition of tbp to the cell solution, (c) a similar shift in the absence of tbp but after ALD-based modification of the electrode surface with ca. 3 Å of alumina, and (d) a shift in current onset by approximately −400 mV when an electrode is modified with both alumina and tbp (i.e., the favorable shifts in the onset potential appear to be additive[68]). We tentatively ascribed the shoulder in the $J-V$ curve for unmodified TiO_2 to the surface-state mediation of the reduction of triiodide, behavior that seemingly can be eliminated either by the addition of tbp or coating with alumina. The simplest interpretation is that both modifiers interact with the sites responsible for mediation and shift their energies to much more negative potentials. (See the discussion in the following sections.) What seems most remarkable is that tbp can engender sizable negative shifts in onset potential even after titanium sites are fully obscured (or nearly so) by alumina.

Figure 6 reveals similar tbp and alumina effects, including roughly additive shifts in voltage for the onset of significant dark current when I_3^- is replaced with $Co(phen)_3^{3+}$ as the electron interceptor. The curves in both figures point to the suppression of electron interception by the redox shuttles rather than shifts in E_{cb} as the primary contributors to enhancements in V_{oc} in corresponding solar cells. Noteworthy is the observation that for modified electrodes the dark currents for $Co(phen)_3^{3+}$ are nearly identical to those for I_3^- (i.e., charge-interception rates and their changes in response to surface modifiers are not significantly dependent on the identity of the redox shuttle).

dx.doi.org/10.1021/la303962y | Langmuir 2013, 29, 806−814

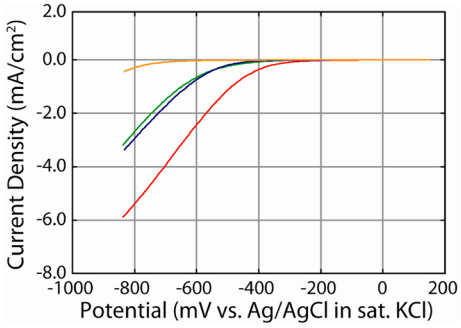

Figure 6. Dark-current-density measurements for flat TiO_2 electrodes using 0.02 M $Co(phen)_3^{3+}$ as the electron interceptor. Key: unmodified electrode (red), after the addition of 0.2 M tbp (green), Al_2O_3-coated electrode with no tbp (blue), and Al_2O_3-coated electrode after the addition of 0.2 M tbp (orange).

Open-Circuit Voltage Decay Measurements. To gain additional insight into how alumina coatings and tbp likely influence photovoltages, we performed open-circuit voltage decay measurements (dark measurements)[69,70] with the starting potential being provided by a potentiostat. These experiments yield plots of the survival time of electrochemically (or photochemically) injected electrons versus the potential of the semiconductor (i.e., E_{Fermi}, relative to a reference electrode). In the absence of dye molecules and photons, injected electrons are removed via interfacial electron transfer to the oxidized form of the redox shuttle. If electrons are transferred solely from the conduction band and if the interfacial electron transfer is rate-determining (as opposed to, say, the rate of thermal population of the conduction band by electrons initially in sub-band-edge states), then a plot of the log of the electron survival time versus the open-circuit potential is expected to be linear.[69,70] In contrast, plots that deviate from linearity would point to the involvement of multiple interception pathways, for example, transfer from nonidentical surface states (defect states) or transfer from both surface states and the conduction band.

Figures 7 and 8 show survival-time plots for various versions of flat TiO_2 in contact with either I_3^- or $Co(phen)_3^{3+}$, respectively. The formal reduction potentials of the two compounds (vs. Ag/AgCl) are +380 and +420 mV, respectively. Because well-designed and highly efficient DSCs typically feature open-circuit photovoltages of ca. 800 to 850

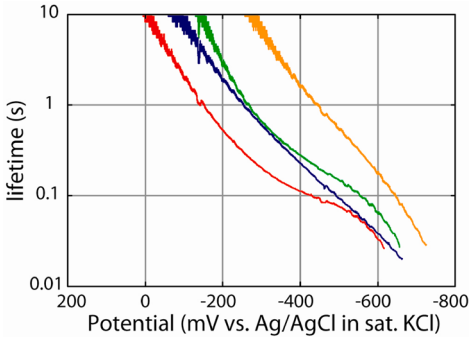

Figure 7. Open-circuit voltage decay plots (electron survival times) for flat TiO_2 electrodes in the presence of 0.02 M I_3^- as the electron interceptor. Key: unmodified electrode (red), after the addition of 0.2 M tbp (green), Al_2O_3-coated electrode with no tbp (blue), and Al_2O_3-coated electrode after the addition of 0.2 M tbp (orange).

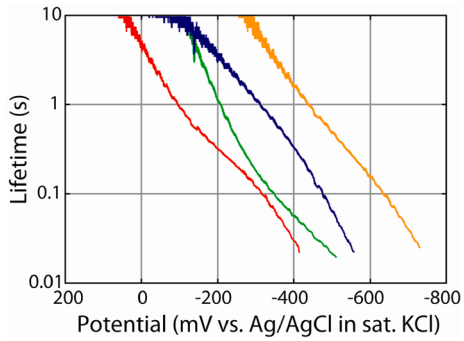

Figure 8. Open-circuit voltage decay plots (electron survival times) for flat TiO_2 electrodes in the presence of 0.02 M $Co(phen)_3^{3+}$ as the electron interceptor. Key: unmodified electrode (red), after the addition of 0.2 M tbp (green), Al_2O_3-coated electrode with no tbp (blue), and Al_2O_3-coated electrode after the addition of 0.2 M tbp (orange).

mV, the regions of greatest practical interest in the decay plots are near −400 mV versus Ag/AgCl. Focusing first on Figure 7, we find that the voltage decay plot for unmodified TiO_2 is curved, implying the participation of surface states in back electron transfer despite the fabrication of the electrode via atomic layer deposition. The addition of tbp increases the survival time (decreases the interception rate) by about a factor of 2 at −400 mV and by a factor of 10 at −160 mV. Notably, however, the plot retains the unusual shape found with the unmodified electrode. Thus, tbp does not appear to passivate surface states, a conclusion not revealed by simple dark-current measurements but consistent with our interpretation above of the Mott−Schottky data.

Electrode modification with ALD alumina elicits a qualitatively different response. The rate of electron interception at a given electrode potential is still slowed, but the decay plot becomes much more nearly linear. Thus, in contrast to tbp, alumina acts to passivate surface states (Figure 3) and presumably drive interception toward primarily a conduction-band pathway. The conclusion regarding passivation is consistent with the findings above for Mott−Schottky experiments. Notably, the decay plots for unmodified and ALD-alumina-modified electrodes converge at ca. −600 mV, suggesting that at this potential a common interception pathway is followed.

The final plot in Figure 7 is for electron transfer to triiodide from a flat TiO_2 electrode modified first with ca. 3 Å of alumina and then with tbp adsorbed from solution. The plot retains the nearly linear shape of the decay plot for the alumina-coated electrode in the absence of tbp, implying that back electron transfer is still mediated by the electrode's conduction band, rather than surface states (defect states). The remarkable effect of tbp is to slow the rate of electron interception by another factor of 7 (at −400 mV).[71] Although a small portion of the tbp-engendered attenuation conceivably could be attributed to the ca. −30 mV shift in E_{cb} brought about by this additive, the majority cannot. A conceivable interpretation is that tbp functions, on both naked and alumina-coated TiO_2, as a physical barrier between the shuttle and the electrode. The resulting increase in electron-transfer distance should lead to less-efficient electron tunneling and, as observed experimentally, a decrease in the electron-transfer rate.

Finally, Figure 8 shows the results of similar experiments, but with the cobalt-containing shuttle molecule. Although not

dx.doi.org/10.1021/la303962y | *Langmuir* 2013, 29, 806−814

identical to those seen with triiodide as the electron acceptor, the results are broadly similar.[69] The addition of alumina yields straighter decay curves, implying the passivation of redox-catalytic surface states. The effect of tbp, however, is somewhat different with the cobalt shuttle versus the iodide shuttle. We lack an explanation for the behavioral difference.

Alternative Adsorbents. Although tbp clearly serves to decrease the rates of electron interception at a given electrode potential (and increase the open-circuit voltage at a given rate of interception), the detailed mechanism of interaction is not clear. We reasoned that replacing tbp with other nitrogen heterocycles might provide mechanistic insight. For simplicity, we limited the investigation of other additives to cells containing $Co(phen)_3^{3+}$ as the electron acceptor and alumina-coated TiO_2 as the electrode. Thus, we chose conditions where surface states appear to be fully passivated and where back electron transfer occurs from the electrode's conduction band. Shown in Figure 9 are plots of dark-current density versus potential in the absence of a nitrogen heterocycle and in the presence of 0.2 M tbp, imidazole, pyridine, 2,6-diphenylpyridine, 2,6-ditert-butylpyridine, or 2,6-lutidine (Chart 1). We

Chart 1. Molecular Structure of Nitrogen-Containing Heterocycles Used to Probe the Mechanistic Behavior of tbp in DSCs

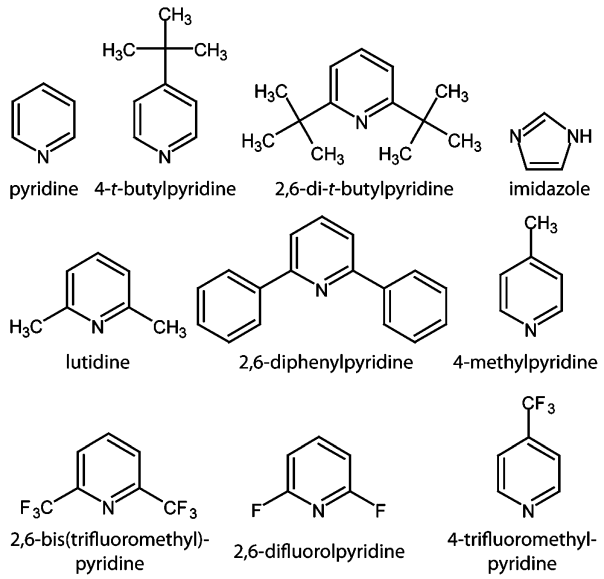

anticipated that the dark-current density at a given potential might correlate with the Lewis basicity of the additive (a proxy for the strength of coordination of a metal atom (e.g., Al(III)) by the heterocycle) or that it might correlate with additive's steric properties. For example, pyridine derivatives substituted at the 2 and 6 sites ought to encounter difficulty in binding to Al(III) sites. Although substantial variations are seen and all additives are suppressed dark currents to some extent, no correlations with heterocycle structural or electronic properties were evident nor were correlations with molecular dipole moments seen

Reasoning that an expanded data set involved a more extreme modulation of heterocycle electronic properties, we examined with a second electrode the effects of added 2,6-difluoropyridine, 4-methylpyridine, 4-trifluoromethylpyridine, 2,6-ditrifluoromethyl-pyridine, and again pyridine and 2,6-lutidine.[72] Again to our surprise, no correlations with heterocycle sterics or electronics were uncovered. Also surprising, as noted above, is the similarity of the tpb-engendered suppression of dark current at electrodes presenting Ti(IV) sites versus electrodes presenting Al(III) sites

An attractive but speculative interpretation is that the heterocycles act not by coordinating titanium or aluminum but by binding to adsorbed lithium ions. The strength of such binding is likely dependent not only on the Lewis basicity of heterocyclic nitrogen atoms but also on the geometry and peripheral electrostatic interaction of substituents (especially 2- and 6-positioned substituents) with the adsorbed and presumably partially solvated lithium cation and, to a lesser extent, with the atoms constituting the electrode surface. Alternatively (and again speculatively), the heterocycles might adsorb in flat orientations rather than normal to the electrode surface. If so, then neither the Lewis basicity of the nitrogen atom nor its accessibility for metal ion coordination would be a governing factor in blocking-layer formation. In principle, quartz crystal microgravimetry studies of photoelectrodes as functions of both lithium salt addition and heterocycle addition should be able to distinguish between these possibilities. These, however, are beyond the scope of the present study.

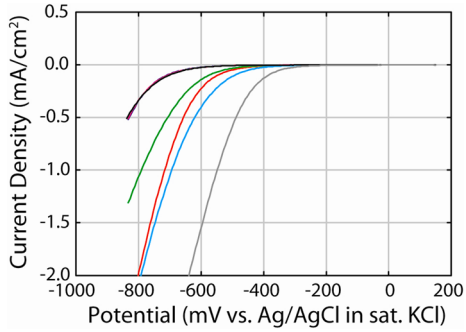

Figure 9. Dark-current-density measurements for flat, alumina-coated TiO_2 electrodes in the presence of 0.02 M $Co(phen)_3^{3+}$ as the electron acceptor. Key to solution additives: no additive (gray), pyridine (light blue), 2,6-diphenylpyridine (red), 2,6-ditert-butylpyridine (green), 2,6-lutidine (pink), tbp (black), and imidazole (blue). Note that the curves for the last three are nearly identical.

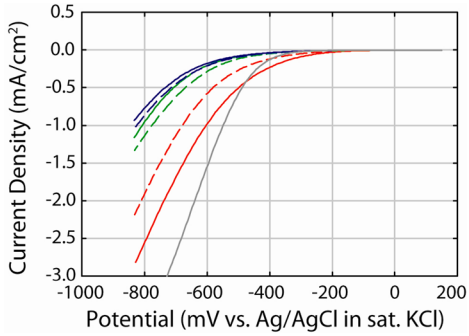

Figure 10. Dark-current-density measurements for flat, alumina-coated TiO_2 electrodes in the presence of 0.02 M $Co(phen)_3^{3+}$ as the electron acceptor. Key to solution additives: no additive (gray), pyridine (red), 2,6-difluoropyridine (red dashed line), 4-methylpyridine (green), 4-trifluoromethylpyridine (green dashed line), 2,6-lutidine (blue), and 2,6-ditrifluoromethylpyridine (blue dashed line).[72].

dx.doi.org/10.1021/la303962y | Langmuir 2013, 29, 806−814

CONCLUSIONS

The fabrication of flat, nonporous, n-type TiO_2 electrodes via atomic-layer deposition has enabled capacitance measurements and the Mott−Schottky analysis to be used to evaluate flat-band potentials, donor densities, and conduction-band-edge energies. Electrode surface modification either by tbp adsorption from solution or by the formation of an ultrathin coating of alumina (∼3 Å) causes only small shifts in E_{fb} and E_{cb} (i.e., ca. −20 to −40 mV). These shifts stand in contrast to much larger additive shifts in onset potentials for the significant flow of dark current. These effects (suppression of dark current) are manifest in DSCs as substantial increases in open-circuit photovoltage.

Measurements of open-circuit voltage decays, when combined with capacitance measurements, show that the striking effects of tbp and ALD-alumina upon onset potentials (i.e., additive shifts of ca. −200 mV for each) have distinctly different causes. Alumina coatings act by passivating surface states (defect states) that otherwise facilitate the interception of injected electrons by redox shuttles. tbp does not passivate surface states and does not shift E_{cb} sufficiently to influence dark-current flow significantly. Instead, adsorbed tbp slows by up to an order of magnitude the rates of interfacial electron transfer, evidently by inhibiting the access of shuttle molecules (electron interceptors) to the electrode surface and diminishing the probability of electron tunnelling (Figure 2). Remarkably, the additive exerts such effects regardless of whether back electron transfer is mediated by surface states or occurs via the electrode's conduction band.

An extension of this study to imidazole, pyridine, and several pyridine derivatives shows that all are effective at suppressing the flow of dark current. However, differences in the extent of dark-current suppression could not be correlated with either the electronic or structural characteristics of the additives. Notably, the most effective additive (lutidine) is methyl-substituted at carbon atoms adjacent to the nitrogen atom, likely preventing the coordination of Ti(IV) or Al(III) atoms on the electrode surface. We speculatively ascribe the remarkable dark-current-inhibition effects instead to the binding of adsorbed lithium ions and the concomitant formation of a surface-blocking layer. In a subsequent report, we will describe how the effects observed at flat electrodes translate mechanistically into efficiency changes in high-area, nanoparticulate, dye-sensitized solar cells.

AUTHOR INFORMATION

Corresponding Author

*E-mail: j-hupp@northwestern.edu.

Author Contributions

This article was written through the contributions of all authors. All authors have given approval to the final version of the article.

Notes

The authors declare no competing financial interest.

ACKNOWLEDGMENTS

We gratefully acknowledge the ANSER Center, an Energy Frontier Research Center funded by the U.S. Department of Energy, Office of Science, Office of Basic Energy Sciences under award number DE-SC0001059, for supporting our work. M.J.K. gratefully acknowledges the NSERC (Canada) for additional support via a postdoctoral fellowship.

REFERENCES

(1) Hagfeldt, A.; Boschloo, G.; Sun, L.; Kloo, L.; Pettersson, H. Dye-sensitized solar cells. *Chem. Rev.* **2010**, *110*, 6595.
(2) Ning, Z.; Fu, Y.; Tian, H. Improvement of dye-sensitized solar cells: what we know and what we need to know. *Energy Environ. Sci.* **2010**, *3*, 1170.
(3) Hamann, T. W.; Jensen, R. A.; Martinson, A. B. F.; Van Ryswyk, H.; Hupp, J. T. Advancing beyond current generation dye-sensitized solar cells. *Energy Environ. Sci.* **2008**, *1*, 66.
(4) Preat, J.; Jacquemin, D.; Perpète, E. A. Towards new efficient dye-sensitised solar cells. *Energy Environ. Sci.* **2010**, *3*, 891.
(5) Grätzel, M. Solar energy conversion by dye-sensitized photovoltaic cells. *Inorg. Chem.* **2005**, *44*, 6841.
(6) Grätzel, M. Photoelectrochemical cells. *Nature* **2001**, 414.
(7) O'Regan, B.; Grätzel, M. A low-cost, high-efficiency solar cell based on dye-sensitized colloidal TiO_2 films. *Nature* **1991**, *353*, 737.
(8) Nazeeruddin, M. K.; Kay, A.; Rodicio, I.; Humphry-Baker, R.; Müller, E.; Liska, P.; Vlachopoulos, N.; Grätzel, M. Conversion of light to electricity by *cis*-X_2bis(2,2′-bipyridyl-4,4′-dicarboxylate)ruthenium(II) charge-transfer sensitizers (X = Cl^-, Br^-, I^-, CN^-, and SCN^-) on nanocrystalline TiO_2 electrodes. *J. Am. Chem. Soc.* **1993**, *115*, 6382.
(9) Nazeeruddin, M. K.; Zakeeruddin, S. M.; Humphry-Baker, R.; Jirousek, M.; Liska, P.; Vlachopoulos, N.; Shklover, V.; Fischer, C.-H.; Grätzel, M. Acid-base equilibria of (2,2′-bipyridyl-4,4′-dicarboxylic acid)ruthenium(II) complexes and the effect of protonation on charge-transfer sensitization of nanocrystalline titania. *Inorg. Chem.* **1999**, *38*, 6298.
(10) Chen, C.-Y.; Wang, M.; Li, J.-Y.; Pootrakulchote, N.; Alibabaei, L.; Ngoc-le, C.-H.; Decoppet, J.-D.; Tsai, J.-H.; Grätzel, C.; Wu, C.-G.; Zakeeruddin, S. M.; Grätzel, M. Highly efficient light-harvesting ruthenium sensitizer for thin-film dye-sensitized solar cells. *ACS Nano* **2009**, *3*, 3103.
(11) Snaith, H. J. Estimating the maximum attainable efficiency in dye-sensitized solar cells. *Adv. Funct. Mater.* **2010**, *20*, 13.
(12) Yella, A.; Lee, H.-W.; Tsao, H. N.; Yi, C.; Chandiran, A. K.; Nazeeruddin, M. K.; Diau, E. W.-G.; Yeh, C.-Y.; Zakeeruddin, S. M.; Grätzel, M. Porphyrin-sensitized solar cells with cobalt (II/III)-based redox electrolyte exceed 12% efficiency. *Science* **2011**, *334*, 629.
(13) Sheng, J.; Hu, L.; Xu, S.; Liu, W.; Mo, L.; Tian, H.; Dai, S. Characteristics of dye-sensitized solar cells based on the TiO_2 nanotube/nanoparticle composite electrodes. *J. Mater. Chem.* **2011**, *21*, 5457.
(14) Haque, S. A.; Palomares, E.; Cho, B. M.; Green, A. N. M.; Hirata, N.; Klug, D. R.; Durrant, J. R. Charge separation versus recombination in dye-sensitized nanocrystalline solar cells: the minimization of kinetic redundancy. *J. Am. Chem. Soc.* **2005**, *127*, 3456.
(15) Boschloo, G.; Hagfeldt, A. Characteristics of the iodide/triiodide redox mediator in dye-sensitized solar cells. *Acc. Chem. Res.* **2009**, *42*, 1819.
(16) Hamann, T. W. The end of iodide? Cobalt complex redox shuttles in DSSCs. *Dalton Trans.* **2012**, 3111.
(17) Daeneke, T.; Kwon, T.-H.; Holmes, A. B.; Duffy, N. W.; Bach, U.; Spiccia, L. High-efficiency dye-sensitized solar cells with ferrocene-based electrolytes. *Nat. Chem.* **2011**, *3*, 211.
(18) Feldt, S. M.; Wang, G.; Boschloo, G.; Hagfeldt, A. Effects of driving forces for recombination and regeneration on the photovoltaic performance of dye-sensitized solar cells using cobalt polypyridine redox couples. *J. Phys. Chem. C* **2011**, *115*, 21500.
(19) Hamann, T. W.; Farha, O. K.; Hupp, J. T. Outer-sphere redox couples as shuttles in dye-sensitized solar cells. Performance enhancement based on photoelectrode modification via atomic layer deposition. *J. Phys. Chem. C* **2008**, *112*, 19756.
(20) Yanagida, S.; Yu, Y.; Manseki, K. Iodine/iodide-free dye-sensitized solar cells. *Acc. Chem. Res.* **2009**, *42*, 1827.
(21) Li, T. C.; Spokoyny, A. M.; She, C.; Farha, O. K.; Mirkin, C. A.; Marks, T. J.; Hupp, J. T. Ni(III)/(IV) bis(dicarbollide) as a fast, noncorrosive redox shuttle for dye-sensitized solar cells. *J. Am. Chem. Soc.* **2010**, *132*, 4580.

(22) Wang, M.; Chamberland, N.; Breau, L.; Moser, J.-E.; Humphry-Baker, R.; Marsan, B.; Zakeeruddin, S. M.; Grätzel, M. An organic redox electrolyte to rival triiodide/iodide in dye-sensitized solar cells. *Nat. Chem.* **2010**, 1.
(23) Klahr, B. M.; Hamann, T. W. Performance enhancement and limitations of cobalt bipyridyl redox shuttles in dye-sensitized solar cells. *J. Phys. Chem. C* **2009**, *113*, 14040.
(24) Spokoyny, A. M.; Li, T. C.; Farha, O. K.; Machan, C. W.; She, C.; Stern, C. L.; Marks, T. J.; Hupp, J. T.; Mirkin, C. A. Electronic tuning of nickel-based bis(dicarbollide) redox shuttles in dye-sensitized solar cells. *Angew. Chem., Int. Ed.* **2010**, *49*, 5339.
(25) Liu, Y.; Jennings, J. R.; Huang, Y.; Wang, Q.; Zakeeruddin, S. M.; Grätzel, M. Cobalt redox mediators for ruthenium-based dye-sensitized solar cells: a combined impedance spectroscopy and near-IR transmittance study. *J. Phys. Chem. C* **2011**, 18847.
(26) Daeneke, T.; Mozer, A. J.; Kwon, T.-H.; Duffy, N. W.; Holmes, A. B.; Bach, U.; Spiccia, L. Dye regeneration and charge recombination in dye-sensitized solar cells with ferrocene derivatives as redox mediators. *Energy Environ. Sci.* **2012**, *5*, 7090.
(27) Jennings, J. R.; Wang, Q. Influence of lithium ion concentration on electron injection, transport, and recombination in dye-sensitized solar cells. *J. Phys. Chem. C* **2010**, *114*, 1715.
(28) Koops, S. E.; O'Regan, B. C.; Barnes, P. R. F.; Durrant, J. R. Parameters influencing the efficiency of electron injection in dye-sensitized solar cells. *J. Am. Chem. Soc.* **2009**, *131*, 4808.
(29) Wang, Z.-S.; Zhou, G. Effect of surface protonation of TiO_2 on charge recombination and conduction band edge movement in dye-sensitized solar cells. *J. Phys. Chem. C* **2009**, *113*, 15417.
(30) Yu, S.; Ahmadi, S.; Sun, C.; Palmgren, P.; Hennies, F.; Zuleta, M.; Göthelid, M. 4-*tert*-Butyl pyridine bond site and band bending on TiO_2(110). *J. Phys. Chem. C* **2010**, *114*, 2315.
(31) Taura, H.; Daiguji, H. Effect of pyridine in electrolyte on the current–voltage characteristics in dye-sensitized solar cells. *Electrochim. Acta* **2010**, *55*, 3491.
(32) Boschloo, G.; Häggman, L.; Hagfeldt, A. Quantification of the effect of 4-*tert*-butylpyridine addition to I^-/I_3^- redox electrolytes in dye-sensitized nanostructured TiO_2 solar cells. *J. Phys. Chem. B* **2006**, *110*, 13144.
(33) Kusama, H.; Orita, H.; Sugihara, H. TiO_2 band shift by nitrogen-containing heterocycles in dye-sensitized solar cells: a periodic density functional theory study. *Langmuir* **2008**, *24*, 4411.
(34) Chandiran, A. K.; Tetreault, N.; Humphry-Baker, R.; Kessler, F.; Baranoff, E.; Yi, C.; Nazeeruddin, M. K.; Grätzel, M. Subnanometer Ga_2O_3 tunnelling layer by atomic layer deposition to achieve 1.1 V open-circuit potential in dye-sensitized solar cells. *Nano Lett.* **2012**, *12*, 3941.
(35) Antila, L. J.; Heikkilä, M. J.; Aumanen, V.; Kemell, M.; Myllyperkiö, P.; Leskelä, M.; Korppi-Tommola, J. E. I. Suppression of forward electron injection from $Ru(dcbpy)_2(NCS)_2$ to nanocrystalline TiO_2 film as a result of an interfacial Al_2O_3 barrier layer prepared with atomic layer deposition. *J. Phys. Chem. Lett.* **2010**, *1*, 536.
(36) Antila, L. J.; Heikkilä, M. J.; Mäkinen, V.; Humalamäki, N.; Laitinen, M.; Linko, V.; Jalkanen, P.; Toppari, J.; Aumanen, V.; Kemell, M.; Myllyperkiö, P.; Honkala, K.; Häkkinen, H.; Leskelä, M.; Korppi-Tommola, J. E. I. ALD grown aluminum oxide submonolayers in dye-sensitized solar cells: the effect on interfacial electron transfer and performance. *J. Phys. Chem. C* **2011**, *115*, 16720.
(37) Prasittichai, C.; Hupp, J. T. Surface modification of SnO_2 photoelectrodes in dye-sensitized solar cells: significant improvements in photovoltage via Al_2O_3 atomic layer deposition. *J. Phys. Chem. Lett* **2010**, *1*, 1611.
(38) Liberatore, M.; Burtone, L.; Brown, T. M.; Reale, A.; Di Carlo, A.; Decker, F.; Caramori, S.; Bignozzi, C. A. On the effect of Al_2O_3 blocking layer on the performance of dye solar cells with cobalt based electrolytes. *Appl. Phys. Lett.* **2009**, *94*, 173113.
(39) Palomares, E.; Clifford, J. N.; Haque, S. A.; Lutz, T.; Durrant, J. R. Control of charge recombination dynamics in dye sensitized solar cells by the use of conformally deposited metal oxide blocking layers. *J. Am. Chem. Soc.* **2003**, *125*, 475.
(40) Fan, S.-Q.; Geng, Y.; Kim, C.; Paik, S.; Ko, J. Correlating the photovoltaic performance of alumina modified dye-sensitized solar cells with the properties of metal-free organic sensitizers. *Mater. Chem. Phys.* **2012**, *132*, 943.
(41) Yu, H.; Xue, B.; Liu, P.; Qiu, J.; Wen, W.; Zhang, S.; Zhao, H. High-performance nanoporous TiO_2/La_2O_3 hybrid photoanode for dye-sensitized solar cells. *ACS Appl. Mater. Interfaces* **2012**, *4*, 1289.
(42) Ganapathy, V.; Karunagaran, B.; Rhee, S.-W. Improved performance of dye-sensitized solar cells with TiO_2/alumina core–shell formation using atomic layer deposition. *J. Power Sources* **2010**, *195*, 5138.
(43) DeVries, M. J.; Pellin, M. J.; Hupp, J. T. Dye-sensitized solar cells: driving-force effects on electron recombination dynamics with cobalt-based shuttles. *Langmuir* **2010**, *26*, 9082.
(44) Bott, A. W. Electrochemistry of semiconductors. *Curr. Sep Drug Dev.* **1998**, *17*, 87.
(45) Gelderman, K.; Lee, L.; Donne, S. W. Flat-band potential of a semiconductor: using the Mott–Schottky equation. *J. Chem. Educ.* **2007**, *84*, 685.
(46) Tan, M. X.; Laibinis, P. E.; Nguyen, S. T.; Kesselman, J. M.; Stanton, C. E.; Lewis, N. S. Principles and applications of semiconductor photoelectrochemistry. *Prog. Inorg. Chem.* **1994**, *41*, 21.
(47) Klahr, B. M.; Martinson, A. B. F.; Hamann, T. W. Photoelectrochemical investigation of ultrathin film iron oxide solar cells prepared by atomic layer deposition. *Langmuir* **2010**, *109*, 13685.
(48) De Gryse, R.; Gomes, W. P.; Cardon, F.; Vennik, J. On the interpretation of Mott-Schottky plots determined at semiconductor/electrolyte systems. *J. Electrochem. Soc.* **1975**, *122*, 711.
(49) Martinson, A. B. F.; Elam, J. W.; Liu, J.; Pellin, M. J.; Marks, T. J.; Hupp, J. T. Radial electron collection in dye-sensitized solar cells. *Nano Lett.* **2008**, *8*, 2862.
(50) Williams, V. O.; Jeong, N. C.; Prasittichai, C.; Farha, O. K.; Pellin, M. J.; Hupp, J. T. Fast transporting ZnO-TiO_2 coaxial photoanodes for dye-sensitized solar cells based on ALD-modified SiO_2 aerogel frameworks. *ACS Nano* **2012**, *12*, 6185.
(51) Jäger, M.; Eriksson, L.; Bergquist, J.; Johansson, O. Synthesis and characterization of 2,6-di(quinolin-8-yl)pyridines. New ligands for bistridentate Ru^{II} complexes with microsecond luminescent lifetimes. *J. Org. Chem.* **2007**, *72*, 10227.
(52) Qiu, S.; Starr, T. L. Zirconium doping in titanium oxide photocatalytic films prepared by atomic layer deposition. *J. Electrochem. Soc.* **2007**, *154*, H472.
(53) Ritala, M.; Leskelä, M.; Niinistö, L.; Haussalo, P. Titanium isopropoxide as a precursor in atomic layer epitaxy of titanium dioxide thin films. *Chem. Mater.* **1993**, *5*, 1174.
(54) Kim, J. Y.; Kim, D.-W.; Jung, H. S.; Hong, K. S. Influence of anatase-rutile phase transformation on dielectric properties of sol-gel derived TiO_2 thin films. *Jpn. J. Appl. Phys.* **2005**, *44*, 6148.
(55) Streetman, B. G. *Solid State Electronic Devices*; Prentice-Hall: New York, 1995.
(56) Jung, H. S.; Kim, H. Origin of low photocatalytic activity of rutile TiO_2. *Electron. Mater. Lett.* **2009**, *5*, 73.
(57) Cantão, M. P.; Cisneros, J. I.; Torresi, R. M. Kinetic study of lithium electroinsertion in titanium oxide thin films. *J. Phys. Chem.* **1994**, *98*, 4865.
(58) Nguyen, P. T.; Anderson, A. R.; Skuo, E. M.; Lund, T. Dye stability and performances of dye-sensitized solar cells with different nitrogen additives at elevated temperatures—Can sterically hindered pyridines prevent dye degradation? *Sol. Energy Mater. Sol. Cells* **2010**, *94*, 1582.
(59) Yin, X.; Zhao, H.; Chen, L.; Tan, W.; Zhang, J.; Weng, Y.; Shuai, Z.; Xiao, X.; Zhou, X.; Li, X.; Lin, Y. The effects of pyridine derivative additives on interface processes at nanocrystalline TiO_2 thin film in dye-sensitized solar cells. *Surf. Interface Anal.* **2007**, *39*, 809.
(60) Göthelid, M.; Yu, S.; Ahmadi, S.; Sun, C.; Zuleta, M. Structure-dependent 4-tert-butyl pyridine-induced band bending at TiO_2 surfaces. *Int. J. Photoenergy* **2011**, *2011*, 401356.
(61) Kaneko, M.; Ueno, H.; Nemoto, J. Schottky junction/ohmic contact behavior of a nanoporous TiO_2 thin film photoanode in

contact with redox electrolyte solutions. *Beilstein J. Nanotechnol.* **2011**, *2*, 127.
(62) Cardon, F.; Gomes, W. P. Semiconductor in contact with a metal or an electrolyte. *J. Phys. D: Appl. Phys.* **1978**, *11*, L63.
(63) Lyon, L. A.; Hupp, J. T. Energetics of the nanocrystalline titanium dioxide/aqueous solution interface: approximate conduction band edge variations between $H_0 = -10$ and $H_- = +26$. *J. Phys. Chem. B* **1999**, *103*, 4623.
(64) Bolts, J. M.; Wrighton, M. S. Correlation of photocurrent-voltage curves with flat-band potential for stable photoelectrodes for the photoelectrolysis of water. *J. Phys. Chem.* **1976**, *80*, 2641.
(65) Li, T. C.; Góes, M. S.; Fabregat-Santiago, F.; Bisquert, J.; Bueno, P. R.; Prasittichai, C.; Hupp, J. T.; Marks, T. J. Surface passivation of nanoporous TiO_2 via atomic layer deposition of ZrO_2 for solid-state dye-sensitized solar cell applications. *J. Phys. Chem. C* **2009**, *113*, 18385.
(66) For high-area nanostructured electrodes, the observed capacitance is usually viewed as being dominated by a chemical capacitance that is sensitive to surface modifications, except via shifts in E_{cb}. Thus, apparent changes in chemical capacitance are often used to gauge and quantify shifts in E_{cb}. Although this strategy presumably is reasonable under most circumstances, it likely will overestimate shifts in E_{cb} if applied in cases where interface modifications that passivate near-band-edge surface states would otherwise contribute to the chemical capacitance. An example may be our recent study of the ALD-zirconia modification of coaxial TiO_2/silica aerogel electrodes. See Li, T. C.; Fabregat-Santiago, F.; Farha, O. K.; Spokoyny, A. M.; Raga, S. R.; Bisquert, J.; Mirkin, C. A.; Marks, T. J.; Hupp, J. T. SiO_2 aerogel templated, porous TiO_2 photoanodes for enhanced performance in dye-sensitized solar cells containing a Ni(III)/(IV) bis-(dicarbollide) shuttle. *J. Phys. Chem. C* **2011**, *115*, 11257.
(67) Martinson, A. B. F.; Góes, M. S.; Fabregat-Santiago, F.; Bisquert, J.; Pellin, M. J.; Hupp, J. T. Electron transport in dye-sensitized solar cells based on ZnO nanotubes: evidence for highly efficient charge collection and exceptionally rapid dynamics. *J. Phys. Chem. A* **2009**, *113*, 4015.
(68) In a few experiments, the effects of changing the concentration of triiodide (from 0.02 to 0.1 or 0.2 M) were examined. Dark currents changed in proportion to the I_3^- concentration.
(69) Zaban, A.; Greenshtein, M.; Bisquert, J. Determination of the electron lifetime in nanocrystalline dye solar cells by open-circuit voltage decay measurements. *ChemPhysChem* **2003**, *4*, 859.
(70) Bisquert, J.; Zaban, A.; Greenshtein, M.; Mora-Seró, I. Determination of rate constants for charge transfer and the distribution of semiconductor and electrolyte electronic energy levels in dye-sensitized solar cells by open-circuit photovoltage decay method. *J. Am. Chem. Soc.* **2004**, *126*, 13550.
(71) A corollary is that for a given electron survival time (or charge interception rate) the addition of tbp elicits an increase in open-circuit potential. Notably, the shifts are of a similar magnitude to the shift in onset potential for the flow of dark current (Figure 5).
(72) A careful comparison of curves for pyridine and for 2,6-lutidine in Figures 9 and 10 reveals differences. These are typical of the degree of electrode-to-electrode variation that we observed. Notably, however, the relative effects of the two additives are paralleled by the two electrodes. Both show a comparatively high degree of dark-current suppression with 2,6-lutidine, with less suppression due to pyridine.